A Multivariable Design Methodology for Voltage Control of a Single-DG-Unit Microgrid

Behrooz Bahrani, *Student Member, IEEE*, Maryam Saeedifard, *Senior Member, IEEE*, Alireza Karimi, *Member, IEEE*, and Alfred Rufer, *Fellow, IEEE*

***Abstract*—This paper proposes a multivariable digital control design methodology for the voltage regulation of an islanded single distributed generation (DG) unit microgrid and its dedicated load. The controller design methodology is based on a family of spectral Multi-Input Multi-Output (MIMO) models of the microgrid system and performs open-loop shaping and system decoupling simultaneously by a convex optimization approach. The control design procedure includes: (i) the determination of a family of nonparametric models of the system at various operating points, (ii) the determination of the class of the controller, and (iii) system open-loop shaping by convex minimization of the summation of the square second norm of the errors between the system open-loop transfer functions and a desired open-loop transfer function. Based on the proposed design methodology, two dq-augmented voltage controllers are proposed to regulate the load voltages of a single-DG-unit microgrid. The proposed controllers guarantee the robust stability and satisfactory dynamic response of the system in spite of load parametric uncertainties and also the presence of nonlinear load. This paper describes the theoretical aspects involved in the design procedure of the controllers and evaluates the performance of the controllers based on simulation studies and experiments.**

***Index Terms*—Convex optimization, digital multivariable control, distributed generation, islanded mode, loop shaping, microgrid, voltage regulation, voltage source converter.**

I. Introduction

CONSISTENT increase in the penetration of distributed generation (DG) units has created significant interest in the optimal grid integration, control, and operation of DG units in the context of microgrids [1]. Microgrids are considered as a basic feature of active distribution networks, able to take full advantage of DG units, if controlled, coordinated, and operated efficiently in both grid-connected and islanded modes [2]–[7].

In the grid-connected mode of operation of a microgrid, the frequency and voltage at the point of common coupling (PCC) are imposed by the utility grid. In this case, each DG unit controls its real/reactive power exchange based on the well-known dq-currents control techniques [2], [3]. In the islanded mode of operation, however, the frequency and voltage are no longer imposed by the grid, and the dq-currents control techniques used in the grid-connected mode cannot guarantee the sustainable operation of the islanded microgrid. Therefore, subsequent to an islanding event, the islanding must be detected as fast as possible [8], and an appropriate control strategy must be adopted to regulate the voltage and frequency of the microgrid and to manage/share the power among the DG units. This paper focuses on the development of a multivariable digital controller design methodology for the voltage control of an islanded single-DG-unit microgrid. Although the proposed design methodology is investigated in the context of a microgrid, it is general and equally applicable for any VSC-based energy conversion application.

The control of an islanded microgrid have been extensively investigated and various control strategies have been proposed [9]–[29]. The most reported strategies are the frequency/real-power and voltage/reactive-power droop-based methods for voltage and frequency control of the islanded microgrids with multiple DG units [1], [10]–[18]. In the context of a single-DG-unit microgrid, several islanded mode control strategies have been proposed and reported [25]–[28]. The control strategy in [25] is intended for a pre-specified, balanced load and cannot accommodate large variations. To enhance the stability and robustness of a microgrid in the presence of balanced and linear load conditions, a linear quadratic Gaussian controller has been proposed in [26]. Reference [27] presents a multivariable controller for voltage regulation of a microgrid with its local RLC load, with uncertain parameters perturbed around their nominal rated values. The control method proposed in [27] leads to a high-order multivariable controller. Although, the designed controller has robust stability to load parameters variations, the performance is guaranteed only for the nominal mode. To accommodate highly unbalanced loads, a control strategy has been proposed in [28] that utilizes an internal oscillator to maintain the frequency and a feedback control system to regulate the voltage. In the presence of nonlinear loads and harmonically polluted load currents, the voltages of a microgrid become severely distorted and the power quality is deteriorated. Consequently, neither of the above-mentioned control strategies can eliminate/minimize the adverse impacts of the harmonics. Furthermore, the robust stability of a microgrid may not be guaranteed for large variations of the load parameters.

This paper proposes a general digital multivariable controller design methodology for the voltage control of a VSC-based system with large variations of the load parameters. The proposed method is based on the system open-loop shaping with a few constraints to ensure the stability of the closed-loop

Manuscript received December 01, 2011; revised February 11, 2012; accepted June 09, 2012. Date of publication October 02, 2012; date of current version January 09, 2013. Paper no. TII-11-0962.

B. Bahrani and A. Rufer are with the Industrial Electronics Laboratory, Ecole Polytechnique Fédérale de Lausanne (EPFL), Lausanne CH-1015, Switzerland (e-mail: behrooz.bahrani@a3.epfl.ch; alfred.rufer@epfl.ch).

M. Saeedifard is with the School of Electrical and Computer Engineering, Purdue University, West Lafayette, IN 47907-2035 USA (e-mail: maryam@ecn.purdue.edu).

A. Karimi is with the Automatic Laboratory, Industrial Electronics Laboratory of Ecole Polytechnique Fédérale de Lausanne (EPFL), Lausanne CH-1015, Switzerland (e-mail: alireza.karimi@epfl.ch).

Color versions of one or more of the figures in this paper are available online at http://ieeexplore.ieee.org.

Digital Object Identifier 10.1109/TII.2012.2221129

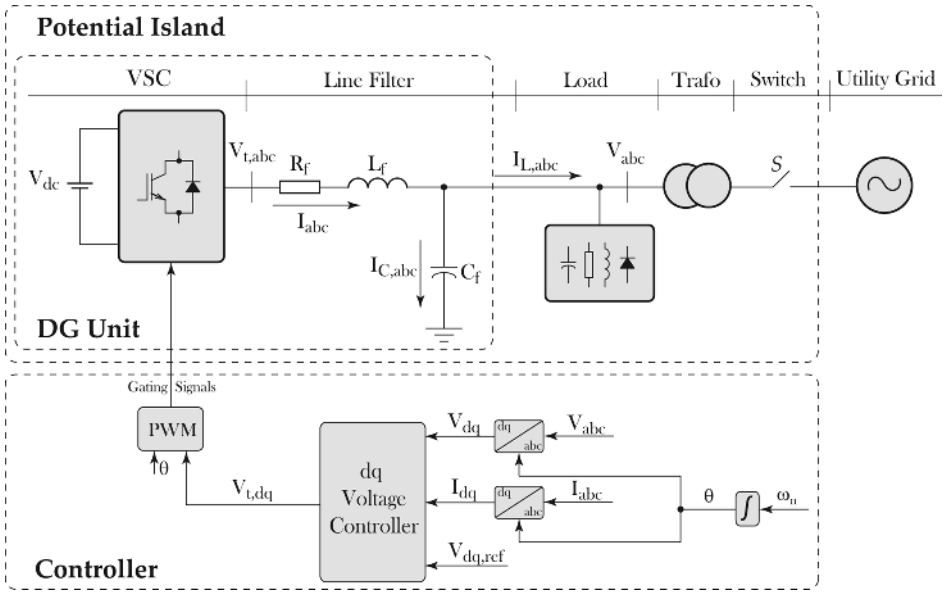

Fig. 1. A single-line diagram of the three-phase test system.

system. It uses multi-input multi-output (MIMO) nonparametric or spectral models of the system for an arbitrary number of desired operating points along with a linearly parameterized MIMO controller to form a set of open-loop transfer function matrices. Based on the dynamic performance and decoupling requirements, a desired open-loop transfer function matrix is formed, and its diagonal and off-diagonal elements are determined. Minimizing the summation of the errors between the open-loop transfer function matrices and the desired one, the coefficients of the controller are determined. The diagonal elements of the controller are tuned to satisfy the desired dynamic performance, while simultaneously, the off-diagonal elements are designed to decouple the dq-axes components. To ensure the stability of the designed controller, the minimization problem is subject to a few constraints. The salient feature of the proposed design methodology, as compared with the existing multivariable controllers, is its capability to accommodate multi-model uncertainties and to achieve robustness with respect to the uncertainties in the load parameters [30].

Based on the proposed design methodology, two novel MIMO dq-augmented control methods, to regulate the voltages of an islanded single-DG unit microgrid, are presented: (i) a PI-based MIMO controller and (ii) PI-based MIMO controller in conjunction with resonant terms, which is able to compensate for the adverse impacts of nonlinear loads. The proposed controllers guarantee robust stability and provide satisfactory performance of the islanded microgrid, despite load uncertainties. The performance of the proposed controllers are studied based on time-domain simulation and are experimentally validated.

The rest of this paper is organized as follows. Section II describes the single-DG unit microgrid study system. Section III presents the proposed multivariable controller design methodology. Section IV presents the details of two designed dq-based voltage controllers for the islanded system. The performance evaluation of the proposed voltage controllers, under various operating scenarios, is reported in Section V. Section VI concludes the paper.

TABLE I
THE PARAMETERS OF THE STUDY SYSTEM OF FIG. 1

Quantity	Value	PU	Comment
R_f	0.3 Ω	0.11	Resistance of VSC Filter
L_f	1.5 mH	0.18	Inductance of VSC Filter
C_f	100 μF	0.074	Capacitance of VSC Filter
S_{base}	0.6 KVA	1	VSC Rated Power
V_{dc}	200 V		DC Bus Voltage
V	40 V (peak)	1	Ph-G Nominal Voltage
f_{sw}	10 kHz		PWM Carrier Frequency
f_s	50 kHz		Sampling Frequency
f	50 Hz		System Nominal Frequency
ω_n	314.15 rad/s		Nominal Angular Frequency

II. STUDY SYSTEM DESCRIPTION

Fig. 1 shows a schematic single-line diagram of the study microgrid system. The microgrid system comprises a single DG unit, which is connected to its dedicated load and the utility grid at the PCC. The DG unit is represented by a DC voltage source, a VSC, and a series LC filter. The filter is realized by an inductor, L_f, and a capacitor, C_f. The inductor has a series internal resistance, R_f. The three-phase load can be any combination of a three-phase parallel RLC load and a three-phase diode rectifier. The microgrid can be connected to the utility grid through a coupling transformer and a switch S. The parameters of the study system of Fig. 1 are summarized in Table I.

In the islanded mode of operation of the system of Fig. 1, which is the main focus of this paper, the switch S is open, and the voltages and frequency at the PCC are no longer imposed by the utility grid. Thus, the primary purpose of the controller block of Fig. 1 is to regulate the amplitude and frequency of the load voltages, V_{abc}. This is achieved by a controller that regulates the dq-components of the load voltages, i.e., V_{dq}, at their desired values. The dq-components of the load voltages along with their corresponding reference values are fed into the controller. The controller then generates the control signals, i.e., the dq-components of the VSC terminal voltages, $V_{t,dq}$. The dq-voltages controller block along with the required input signals and their associated output signals are also depicted in Fig. 1. As shown

in Fig. 1, the frequency of the islanded microgrid is set at the system nominal frequency, ω_n.

In Section III, a multivariable design methodology for the voltage control of the system of Fig. 1 is proposed.

III. The Proposed Multivariable Control Design Methodology

This section proposes a general methodology to design a voltage controller for a VSC-based system. The proposed methodology originates from the MIMO controller design approach in [30], which based on a family of spectral MIMO models of the system, develops a convex optimization-based control method. The basic idea of the proposed approach is to shape the open-loop transfer function matrix of the system by minimizing the absolute errors between a family of the open-loop transfer function matrices of the system, obtained for various operating points of interest, i.e., $\mathscr{L}=\{\mathbf{L_i}(j\omega); i=1,\ldots,m; \omega\in\mathbb{R}\}$, and a desired open-loop transfer function matrix, i.e., $\mathbf{L_d}(s)$. The system open-loop transfer function matrix at the ith operating point of the system is $\mathbf{L_i}(j\omega) = \mathbf{G_i}(j\omega)\mathbf{K}(j\omega)$, where $\mathbf{G_i}(j\omega)$ represents the system transfer function matrix at the ith operating point of the system, and $\mathbf{K}(j\omega)$ represents the controller transfer function matrix. Since this loop shaping approach does not necessarily guarantee the desired performance and stability of the closed-loop system, to meet performance and robustness specifications, the minimization problem is subject to a few constraints. In Section IV, the detailed design procedure of the controller is described. The procedure includes the following main steps: (i) the determination of a family of the nonparametric models of the system at various operating points, (ii) the determination of the class of the controller, and (iii) system open-loop shaping by the minimization of the summation of the square second norm of the errors between the system open-loop transfer function matrices and a desired open-loop transfer function matrix.

A. Determination of a Family of Nonparametric Models

Assuming a system with two inputs and two outputs, the transfer function matrix of the system at each operating point, based on nonparametric models, is given by:

$$\mathbf{G_i}(j\omega)=\begin{bmatrix} G_{i,11}(j\omega) & G_{i,12}(j\omega)\\ G_{i,21}(j\omega) & G_{i,22}(j\omega)\end{bmatrix} \tag{1}$$

where index i represents the ith operating point of the system. The elements of the matrix $\mathbf{G_i}(j\omega)$ are determined by frequency response measurements of the system, i.e., the estimation of the frequency response of the system in the range of the frequencies of interest. To achieve this, a potential approach is to stimulate the system by using a pseudo-random binary sequence (PRBS) generator at its input ports [32] and measure the response at the output ports. A PRBS, as depicted in Fig. 2, is a sequence of pulses with random width and a pre-specified amplitude, which has the properties of a discrete-time white noise (a flat spectrum) and has special mathematical characteristics that make it attractive as a stimulus signal [32]. Considering the system of Fig. 1, the dq-components of the VSC voltages, $V_{t,d}$ and $V_{t,q}$, are assumed as the two inputs and the dq-components of the load voltages, V_d and V_q, as the two outputs at the ith operating point. Applying a PRBS with a sufficient amplitude, within the operating range of the system, to $V_{t,d}$, two elements of the matrix $\mathbf{G_i}$ can be identified as follows:

$$G_{i,11}(j\omega)=\frac{\mathscr{F}(V_d)}{\mathscr{F}(V_{t,d})} \quad \text{and} \quad G_{i,21}(j\omega)=\frac{\mathscr{F}(V_q)}{\mathscr{F}(V_{t,d})} \tag{2}$$

where $\mathscr{F}$ represents the Fourier transform. Likewise, by applying a PRBS to $V_{t,q}$, the other two elements of the matrix $\mathbf{G_i}$ can be identified as:

$$G_{i,12}(j\omega)=\frac{\mathscr{F}(V_d)}{\mathscr{F}(V_{t,q})} \quad \text{and} \quad G_{i,22}(j\omega)=\frac{\mathscr{F}(V_q)}{\mathscr{F}(V_{t,q})}. \tag{3}$$

Repeating the same procedure for m operating points, a family of the nonparametric models of the system are determined as:

$$\mathscr{G}=\{\mathbf{G_i}(j\omega); i=1,\ldots,m; \omega\in\mathbb{R}\}. \tag{4}$$

The family of the nonparametric models of the system of Fig. 1, represented by (4), are used as a basis to design the voltage controllers. It must be noted that if the parametric model of the system is available, one can extract the frequency response of the parametric model for various operating points to form the required spectral model family. However, since parametric models do not precisely reflect the dynamic behavior of the system, the PRBS-based identification approach is preferred.

B. Determination of the Class of Controller

To form the open-loop transfer function matrix of the overall system including the controller, the class of the to-be-designed controller is required. Since the objective is to design a linearly parameterized multivariable digital controller, the class of the controller is determined in the z-domain. A generic form of such a multivariable discrete-time controller in the z-domain is given by:

$$\mathbf{K}(j\omega)=\begin{bmatrix} K_{11}(j\omega) & K_{12}(j\omega)\\ K_{21}(j\omega) & K_{22}(j\omega)\end{bmatrix}. \tag{5}$$

Each element of the controller matrix of (5) is then given by:

$$K_{ij}(j\omega,\rho)=\rho^T\phi(j\omega) \tag{6}$$

where

$$\rho^T=[\rho_0,\rho_1,\rho_2,\ldots,\rho_n] \tag{7}$$

and $\phi(j\omega)$ is the frequency response of

$$\phi^T(z)=[\phi_1(z),\phi_2(z),\ldots,\phi_n(z)] \tag{8}$$

computed by replacing $z=e^{-j\omega}$. In (7) and (8), n is the number of the controller parameters for each element of the controller matrix, and $\phi_\omega(z)$, $\omega=1,\ldots,n$, are the stable transfer functions possibly with poles on the imaginary axis. Therefore, the 2×2 controller of (5) has $4\times n$ controller parameters, which must be determined.

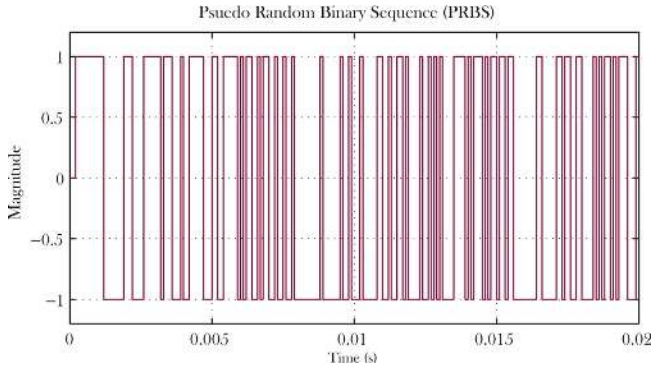

Fig. 2. A typical PRBS in the time domain.

Having the family of the nonparametric models of the system from (4) and the defined controller class from (5), a family of the open-loop transfer function matrices of the overall system is concluded by:

$$\mathscr{L} = \{\mathbf{L_i}(j\omega); i = 1, \ldots, m; \omega \in \mathbb{R}\} \tag{9}$$

in which $\mathbf{L_i}(j\omega) = \mathbf{G_i}(j\omega)\mathbf{K}(j\omega)$.

C. Loop Shaping by Convex Optimization

The loop shaping of the open-loop transfer function matrix of a system with a family of nonparametric models like $\mathscr{L}$ is carried out by minimizing the summation of the square second norm of the errors between the individual entries of $\mathscr{L}$ and a desired open-loop transfer function matrix, $\mathbf{L_D}(s)$. Consequently, the control design procedure turns to an optimization problem as follows [30]:

$$\min_{\rho} \sum_{i=1}^{m} \parallel \mathbf{L_i}(\rho) - \mathbf{L_D} \parallel^2 \tag{10}$$

where m is the number of the open-loop transfer function matrices that form the family of $\mathscr{L}$. The desired open-loop transfer function matrix, $\mathbf{L_D}$, is chosen to meet the system requirements, e.g., satisfactory dynamic response and reduced coupling between the outputs. As an example, for a 2×2 MIMO system, a potential desired open-loop transfer function matrix is:

$$\mathbf{L_D}(s) = \begin{bmatrix} L_{D1}(s) & 0 \\ 0 & L_{D2}(s) \end{bmatrix} = \begin{bmatrix} \frac{\omega_c}{s} & 0 \\ 0 & \frac{\omega_c}{s} \end{bmatrix}. \tag{11}$$

In the transfer function matrix of (11), the off-diagonal elements are set to zero to decouple the system while the diagonal elements are tuned to provide required dynamic response by adjusting ω_c. Furthermore, the closed-loop sensitivity function of the diagonal elements, $S = (1 + L_{i,qq})^{-1}$, can be shaped using $W_1(j\omega)S(j\omega) < 1 \ \forall \ \omega$, where $W_1(j\omega)$ is a weighting filter. This is an H_∞ performance condition that guarantees the robustness of the main axes [31]. A convex approximation of this condition can be given by the following linear constraints [30]:

$$\begin{aligned} &|W_1(j\omega)[1 + L_{Dq}(j\omega, \rho)]| \\ &\quad - \mathcal{R}e\{[1 + L_{Dq}(-j\omega)][1 + L_{i,qq}(j\omega, \rho)]\} < 0 \\ &\quad \forall\, \omega \in \mathbb{R},\ i = 1, \ldots, m, \text{ and } q = 1, 2. \end{aligned} \tag{12}$$

Solving the optimization problem of (10) constrained to (12) results in a decoupled open-loop transfer function matrix, which provides satisfactory reference tracking capability. However, it does not guarantee the stability of the multivariable closed-loop system. To ensure the stability of the multivariable closed-loop system, the Generalized Nyquist Stability criterion must be respected. This criterion guarantees the stability of the feedback system *if and only if the net sum of counterclockwise encirclements of the critical point* $(-1 + j0)$ *by the set of eigenvalues of the matrix* $\mathbf{L_i}(j\omega)$ *is equal to the total number of the right-half plane poles of* $\mathbf{L_i}(s)$. To satisfy this condition, adopting *Gershgorin bands*, reference [30] proves that assuming the nonparametric model $\mathbf{G_i}(j\omega)$, the linearly parameterized controller $\mathbf{K}(z)$ defined in (6) stabilizes the closed-loop system if:

$$\begin{aligned} &r_{i,q}(\omega, \rho) \\ &\quad - \frac{\mathcal{R}e\{[1 + L_{Dq}(-j\omega)][1 + L_{i,qq}(j\omega, \rho)]\}}{|1 + L_{Dq}(j\omega)|} < 0 \\ &\quad \forall\, \omega \text{ for } i = 1, \ldots, m \text{ and } q = 1, 2. \end{aligned} \tag{13}$$

In (13), the diagonal matrix $\mathbf{L_D}(j\omega)$ should be chosen such that the number of counterclockwise encirclements of the critical point by the Nyquist plot of the set of its eigenvalues is equal to the number of unstable poles of $\mathbf{G_i(s)}$. For example, the transfer function matrix of (11) is a fulfilling choice. Moreover, $r_{i,1}(\omega, \rho)$ and $r_{i,2}(\omega, \rho)$ are defined as:

$$r_{i,1}(\omega, \rho) = |L_{i,21}(j\omega, \rho)| \tag{14}$$

and

$$r_{i,2}(\omega, \rho) = |L_{i,12}(j\omega, \rho)|. \tag{15}$$

Considering the constraints for the desired performance given by (12) and the constraints for the stability of the closed-loop system given by (13), the design procedure is summarized into the following optimization problem:

$$\min_{\rho} \sum_{i=1}^{m} \parallel \mathbf{L_i}(\rho) - \mathbf{L_D} \parallel^2 \tag{16}$$

subject to

$$\begin{aligned} &|W_1(j\omega)[1 + L_{Dq}(j\omega, \rho)]| \\ &\quad - \mathcal{R}e\{[1 + L_{Dq}(-j\omega)][1 + L_{i,qq}(j\omega, \rho)]\} < 0 \\ &\quad \forall\, \omega \in \mathbb{R} \text{ for } i = 1, \ldots, m \text{ and } q = 1, 2. \end{aligned} \tag{17}$$

and

$$\begin{aligned} &r_{i,q}(\omega, \rho) \\ &\quad - \frac{\mathcal{R}e\{[1 + L_{Dq}(-j\omega)][1 + L_{i,qq}(j\omega, \rho)]\}}{|1 + L_{Dq}(j\omega)|} < 0 \\ &\quad \forall\, \omega \in \mathbb{R} \text{ for } i = 1, \ldots, m \text{ and } q = 1, 2. \end{aligned} \tag{18}$$

The optimization problem of (16), known as a *semi-infinite programming* (SIP) problem, includes infinite number of constraints and finite number of variables, which is difficult to solve. A practical solution to this problem is to neglect the frequencies above a certain frequency, i.e., $\omega_{\max}$, for which the gain of the open-loop transfer function matrix is close to zero. For discrete-time systems, this frequency can be chosen as the Nyquist frequency. Then, one can only consider the

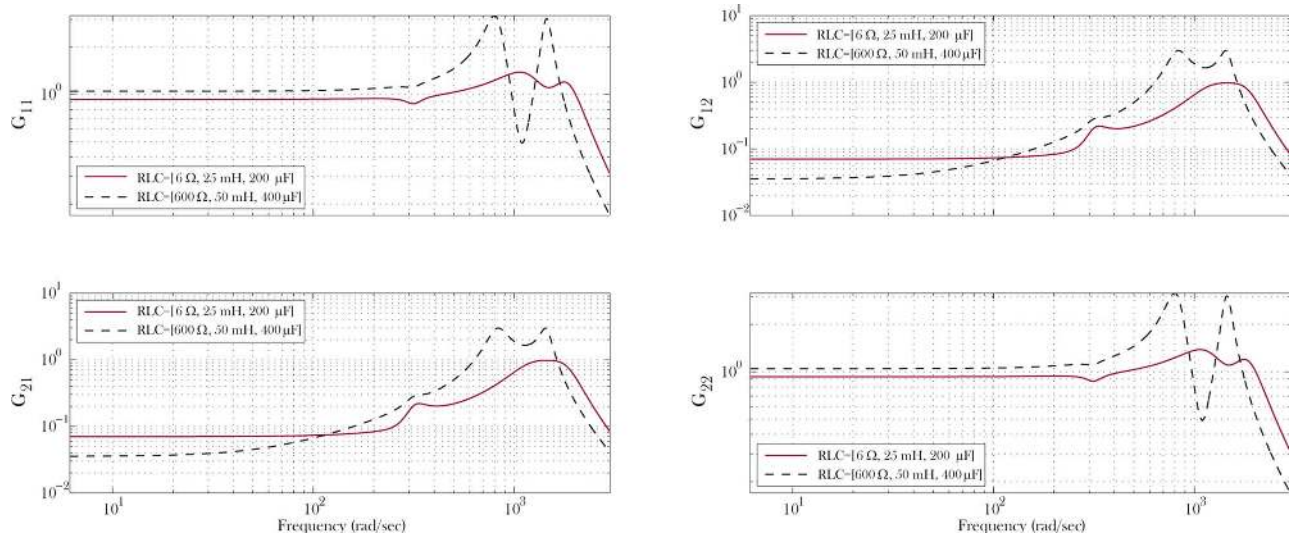

Fig. 3. Two spectral models of the system corresponding to $RLC = [6\ \Omega,\ 25\ \text{mH},\ 200\ \mu\text{F}]$ and $RLC = [600\ \Omega,\ 50\ \text{mH},\ 400\ \mu\text{F}]$.

gridded frequency interval $[0\ \omega_{\max}]$, which contains finite frequency points. Such problems are referred to as *semi-definite programming* (SDP) problems and are solved utilizing standard SDP-solvers, e.g., SeDuMi [33].

Choosing N linearly spaced frequencies within the range of $[0\ \omega_{\max}] \in \mathbb{R}$, the quadratic objective function is approximated by:

$$\sum_{i=1}^{m} \parallel \mathbf{L_i}(\rho) - \mathbf{L_D} \parallel^2 \approx \sum_{i=1}^{m}\sum_{k=1}^{N} \parallel \mathbf{L_i}(j\omega_k, \rho) - \mathbf{L_D}(j\omega_k) \parallel_F \tag{19}$$

where $\parallel \cdot \parallel_F$ is the Frobenius norm. Therefore, the following optimization problem is deduced:

$$\min_{\rho} \sum_{i=1}^{m}\sum_{k=1}^{N} \parallel \mathbf{L_i}(j\omega_k, \rho) - \mathbf{L_D}(j\omega_k) \parallel_F \tag{20}$$

subject to

$$|W_1(j\omega_k)[1 + L_{Dq}(j\omega_k)]| - \mathcal{R}e[1 + L_{Dq}(-j\omega_k)][1 + L_{i,qq}(j\omega_k, \rho)] < 0 \tag{21}$$

and

$$r_{i,q}(\omega_k, \rho) - \frac{\mathcal{R}e\{[1 + L_{Dq}(-j\omega_k)][1 + L_{i,qq}(j\omega_k, \rho)]\}}{|1 + L_{Dq}(j\omega_k)|} < 0 \quad \text{for } k = 1, \ldots, N,\ i = 1, \ldots, m, \text{ and } q = 1, 2. \tag{22}$$

The optimization problem of (20) in conjunction with the constraints in (22) and (21) is used as a basis to determine the coefficients of the MIMO controller, which is the subject of Section IV.

IV. The Proposed dq-Augmented Voltage Controllers

In this section, the aforementioned spectral-model-based multivariable control design approach of Section III is used to propose two dq-based voltage control strategies for the single-DG-unit islanded microgrid of Fig. 1: (i) a multivariable-PI voltage controller (MPVC) comprising four PI-controllers to regulate the load voltages in the presence of linear, three-phase, balanced loads and (ii) a multivariable-PI-resonant voltage controller (MPRVC), which uses resonant terms in conjunction with the PI-controllers of the MPVC to regulate the load voltages in the presence of linear and/or nonlinear loads.

A. Multivariable-PI Voltage Controller

Based on the design methodology of Section III, the first step is to obtain the nonparametric models of the system at the operating points for which the controller is designed. Assuming the uncertainty ranges the RLC load parameters, the spectral models corresponding to the extreme points of the assumed ranges are taken. The assumed ranges are presented by

$$\begin{aligned} 6\ \Omega \le R \le 600\ \Omega \\ 25\ \text{mH} \le L \le 50\ \text{mH} \\ 200\ \mu\text{F} \le C \le 400\ \mu\text{F}. \end{aligned} \tag{23}$$

Therefore, eight models corresponding to the vertices of the cube formed by the assumed ranges in a three-dimensional space are utilized in the optimization problem. Fig. 3 depicts two of the assumed models corresponding to $RLC = [6\ \Omega,\ 25\ \text{mH},\ 200\ \mu\text{F}]$ and $RLC = [600\ \Omega,\ 50\ \text{mH},\ 400\ \mu\text{F}]$. It should be noted that as far as the optimization problem is feasible and has a solution, any desired number of models can be utilized in the optimization problem.

The second step is to determine the class of the controller. The primary goal of the MPVC is to stabilize the system and to regulate the voltages in the presence of three-phase, balanced, linear loads. Therefore, four PI-controllers are selected for the individual elements of the transfer function matrix of the MIMO controller. Fig. 4 depicts the structure of the MPVC. The proportional and integrator coefficients of the individual PI-controllers are determined in the third step of the control design methodology, i.e., solving the constrained minimization problem. To solve the constrained minimization problem of (20), the desired

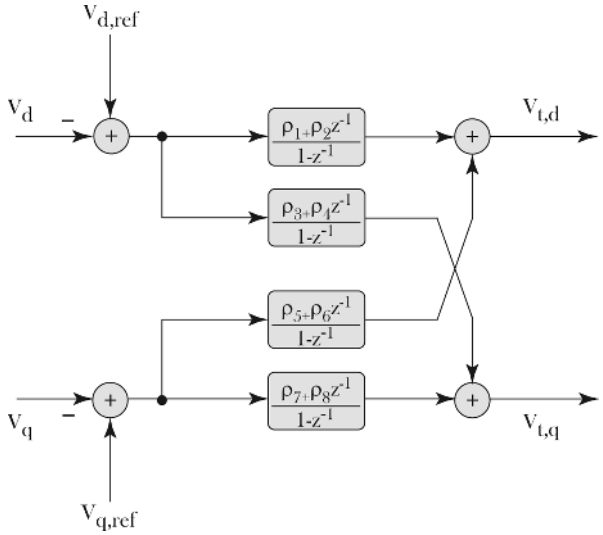

Fig. 4. The structure of the MPVC.

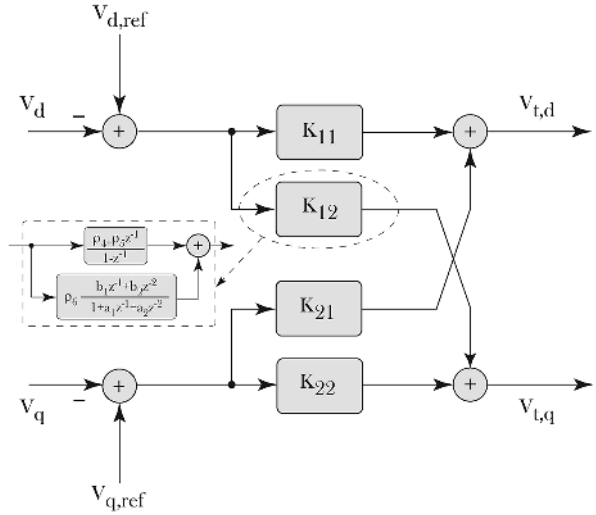

Fig. 5. The structure of the MPRVC.

open-loop transfer function matrix is required. A reasonable open-loop transfer function matrix for this application is considered as:

$$\mathbf{L_D}(s) = \begin{bmatrix} \frac{\omega_c}{s} & 0 \\ 0 & \frac{\omega_c}{s} \end{bmatrix} \tag{24}$$

where $\omega_c = 150$ rad/s. The zero off-diagonal elements of $\mathbf{L_D}$ are to decouple the $d-$ and q-axes. Solving the minimization problem of (20), the controller transfer function matrix is calculated as:

$$\begin{aligned} \mathbf{K}(z) &= \begin{bmatrix} \frac{\rho_1+\rho_2 z^{-1}}{1-z^{-1}} & \frac{\rho_3+\rho_4 z^{-1}}{1-z^{-1}} \\ \frac{\rho_5+\rho_6 z^{-1}}{1-z^{-1}} & \frac{\rho_7+\rho_8 z^{-1}}{1-z^{-1}} \end{bmatrix} \\ &= \begin{bmatrix} \frac{0.061-0.058 z^{-1}}{1-z^{-1}} & \frac{0.048-0.048 z^{-1}}{1-z^{-1}} \\ \frac{-0.048+0.048 z^{-1}}{1-z^{-1}} & \frac{0.061-0.059 z^{-1}}{1-z^{-1}} \end{bmatrix}. \end{aligned} \tag{25}$$

B. Multivariable-PI-Resonant Voltage Controller

The MPVC in Section IV-A is designed based on the assumption of having three-phase, balanced, linear loads. In the presence of nonlinear loads where the currents are significantly polluted with low-order harmonics, the designed MPVC does not provide satisfactory performance. The objective of this section is to improve the performance of the MPVC by modifying the class of the controller and adding additional resonant terms to the individual PI-controllers and also to the desired open-loop transfer function matrix. The structure of the modified MPVC in conjunction with the resonant terms, i.e., the so-called MPRVC, is depicted in Fig. 5. The harmonics of the order of 5 and 7 in the abc-frame both appear at the frequency of 300 Hz in the dq-frame. Therefore, adding a single resonant term tuned at the frequency of 300 Hz can eliminate both 5th and 7th voltage harmonics. As an example, the second diagonal element of the controller transfer function matrix, i.e., $K_{12}(z)$, is expressed as

$$K_{12}(z) = \frac{\rho_4 + \rho_5 z^{-1}}{1 - z^{-1}} + \rho_6 \frac{b_1 z^{-1} + b_2 z^{-2}}{1 + a_1 z^{-1} + a_2 z^{-2}}. \tag{26}$$

The term $b_1 z^{-1} + b_2 z^{-2}/1 + a_1 z^{-1} + a_2 z^{-2}$ in (26) represents an equivalent term for $\omega_h^2/s^2 + 2\zeta\omega_h s + \omega_h^2$ in discrete-time domain, in which $\omega_h = 2\pi 300$, and $\zeta = 3/\omega_h$ is the damping ratio. The coefficients a_1, a_2, b_1, and b_2 are determined as follow:

$$\begin{aligned} b_1 &= 1 - \alpha(\beta + \frac{\zeta\omega_h}{\omega_b}\eta) \\ b_2 &= \alpha^2 + \alpha(\frac{\zeta\omega_h}{\omega_b}\eta - \beta) \\ a_1 &= -2\alpha\beta \\ a_2 &= \alpha^2 \end{aligned} \tag{27}$$

in which $\omega_b = \omega_h\sqrt{1-\zeta^2}$ for $\zeta < 1$, $\alpha = e^{-\zeta\omega_h T_s}$, $\beta = \cos(\omega_b T_s)$, $\eta = \sin(\omega_b T_s)$, and T_s represents the sampling period. Note that in case the elimination of higher order harmonics, e.g., 11th and 13th harmonic voltage components, is also of interest, additional resonant terms can be added to the existing terms.

To determine the coefficients of the MPRVC, similar to the design procedure of the MPVC, the identified spectral models of the system are required. Similar to the MPVC, eight spectral models, corresponding to the vertices of the cube formed by the intervals of (23), are obtained and utilized in the design procedure. Moreover, the desired open-loop transfer function matrix is determined by adding resonant terms tuned at 300 Hz to the diagonal elements of the transfer function matrix of (24). Therefore, the desired open-loop transfer function matrix is:

$$\mathbf{L_D}(s) = \begin{bmatrix} \frac{\omega_{c1}}{s} + \frac{\omega_{c2}}{s^2+2\zeta\omega_h s+\omega_h^2} & 0 \\ 0 & \frac{\omega_{c1}}{s} + \frac{\omega_{c2}}{s^2+2\zeta\omega_h s+\omega_h^2} \end{bmatrix} \tag{28}$$

in which $\omega_{c1} = 70$ rad/s. Moreover, ω_{c2} for the models with $R = 6\ \Omega$ is 90000 rad/s and for the models with $R = 600\ \Omega$ is 80000 rad/s. Then, solving the optimization problem of (20), the coefficients of the MPRVC are determined and expressed by (29) at the bottom of the following page.

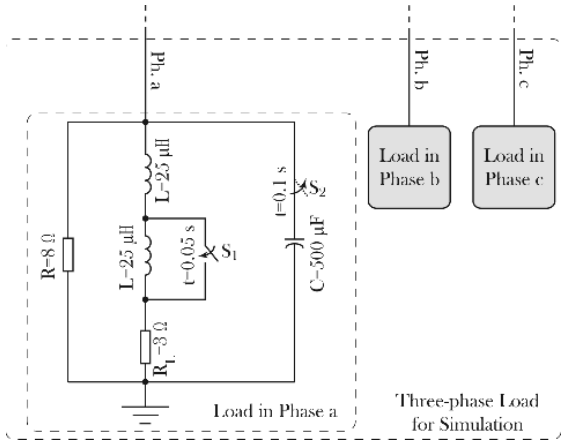

Fig. 6. Three-phase linear load for the inductive-capacitive load change scenarios.

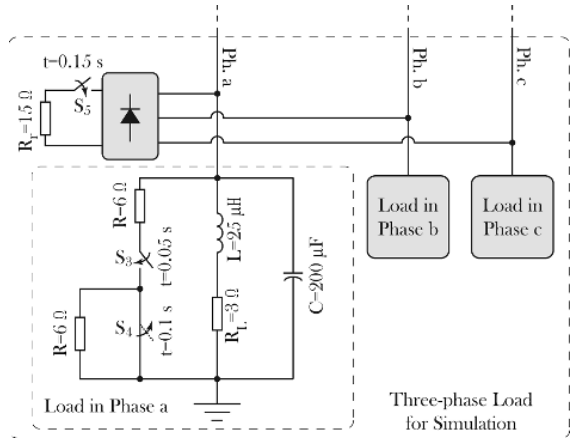

Fig. 7. Three-phase nonlinear load for the resistive-load change scenarios.

V. Performance Evaluation

This section presents a set of simulation and experimental results to evaluate and validate the performance of the proposed controllers for the microgrid system of Fig. 1.

A. Simulation Results

This section reports the simulation studies of the single-DG-unit microgrid system of Fig. 1, based on the proposed MPVC and MPRVC, in the MATLAB/PLECS environment. The simulation studies are conducted to demonstrate the performance of the proposed controllers under two load change scenarios: (i) inductive-capacitive load changes and (ii) linear and nonlinear resistive load changes. For the former, the RLC load parameters as well as their arrangement are chosen based on the three-phase balanced RLC load of Fig. 6 while for the latter, the three-phase load of Fig. 7, which includes both linear and nonlinear resistive loads, is used.

It must be noted that in the following tests, the results are shown starting from the time instant $t = 0$ s. However, $t = 0$ s does not correspond to the start-up instant of the converter.

1) Inductive-Capacitive Load Change: Initially, the system of Fig. 1 operates in the islanded mode and the three-phase load of Fig. 6 is connected at the PCC. The MPVC is in service, and the dq-components of the load voltages are respectively regulated at 40 V and 0 V. The switches S_1 and S_2 in Fig. 6 are closed at $t = 0.05$ s and $t = 0.1$ s, respectively. This corresponds to two load changes, i.e., an inductive and a capacitive load change.

Fig. 8 shows the dynamic response of the islanded system to the load changes. The load voltages are depicted in Fig. 8(a). The corresponding d- and q-components of the load voltages are shown in Fig. 8(b), which during and subsequent to the load changes are regulated at 40 V and 0 V, respectively, by the MPVC. The d- and q-components of the VSC ac-side currents are shown in Fig. 8(c), which after each load change, are changed accordingly to accommodate the load demand requirements. Subsequent to each load change, the MPVC adjusts the d- and q-components of the VSC terminal voltages at their corresponding new values, as depicted in Fig. 8(d).

The simulation results of a similar case study, when the MPRVC is in service, are also shown in Fig. 9. In the presence of linear three-phase loads, both controllers act in a similar way. This is due to the absence of any harmonic distortion in the system. The difference between the performance of the MPVC and MPRVC is highlighted in Section V-A2, where significant low-order harmonic currents and consequently voltages flow in the system. The simulation results of Figs. 8 and 9 verify the robust stability and the performance of both proposed controllers with respect to the balanced, linear load parameter uncertainties.

2) Resistive Load Changes: To evaluate the performance of the proposed controllers upon the change of resistive loads, the system is loaded with the three-phase load of Fig. 7. As shown in Fig. 7, the system is subject to three resistive load changes. At $t = 0.05$ s, a three-phase purely resistive load of 6 Ω is connected in parallel to the load. This resistive load is stepped up from 6 Ω to 12 Ω at $t = 0.1$ s. Then, at $t = 0.15$ s, a three-phase rectifier, with a resistive load of 15 Ω, is paralleled to the RLC load.

Figs. 10 and 11 show the responses of the system to the load changes when the MPVC and the MPRVC are, respectively, in service. Figs. 10(a) and 11(a) show the instantaneous load voltages, which are regulated at their reference values during and

$$\mathbf{K}(z) = \begin{bmatrix} \frac{\rho_1+\rho_2 z^{-1}}{1-z^{-1}} + \frac{\rho_3(b_1 z^{-1}+b_2 z^{-2})}{1+a_1 z^{-1}+a_2 z^{-2}} & \frac{\rho_4+\rho_5 z^{-1}}{1-z^{-1}} + \frac{\rho_6(b_1 z^{-1}+b_2 z^{-2})}{1+a_1 z^{-1}+a_2 z^{-2}} \\ \frac{\rho_7+\rho_8 z^{-1}}{1-z^{-1}} + \frac{\rho_9(b_1 z^{-1}+b_2 z^{-2})}{1+a_1 z^{-1}+a_2 z^{-2}} & \frac{\rho_{10}+\rho_{11} z^{-1}}{1-z^{-1}} + \frac{\rho_{12}(b_1 z^{-1}+b_2 z^{-2})}{1+a_1 z^{-1}+a_2 z^{-2}} \end{bmatrix}$$
$$= \begin{bmatrix} \frac{0.061-0.059 z^{-1}}{1-z^{-1}} + \frac{-0.012(b_1 z^{-1}+b_2 z^{-2})}{1+a_1 z^{-1}+a_2 z^{-2}} & \frac{0.030-0.030 z^{-1}}{1-z^{-1}} + \frac{-0.001(b_1 z^{-1}+b_2 z^{-2})}{1+a_1 z^{-1}+a_2 z^{-2}} \\ \frac{-0.030+0.030 z^{-1}}{1-z^{-1}} + \frac{0.001(b_1 z^{-1}+b_2 z^{-2})}{1+a_1 z^{-1}+a_2 z^{-2}} & \frac{0.061-0.059 z^{-1}}{1-z^{-1}} + \frac{-0.012(b_1 z^{-1}+b_2 z^{-2})}{1+a_1 z^{-1}+a_2 z^{-2}} \end{bmatrix}. \quad (29)$$

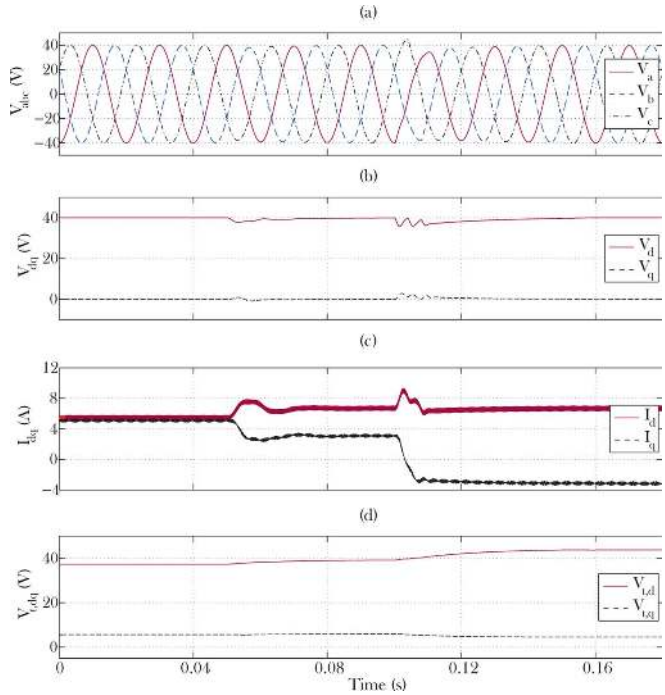

Fig. 8. The simulation response of the islanded system of Fig. 1 to the two-step inductive-capacitive load change of Fig. 6 when the MPVC is in service: (a) the three-phase load voltages, (b), (c), and (d) the d- and q-components of the load voltages, the VSC ac-side currents, and the VSC terminal voltages.

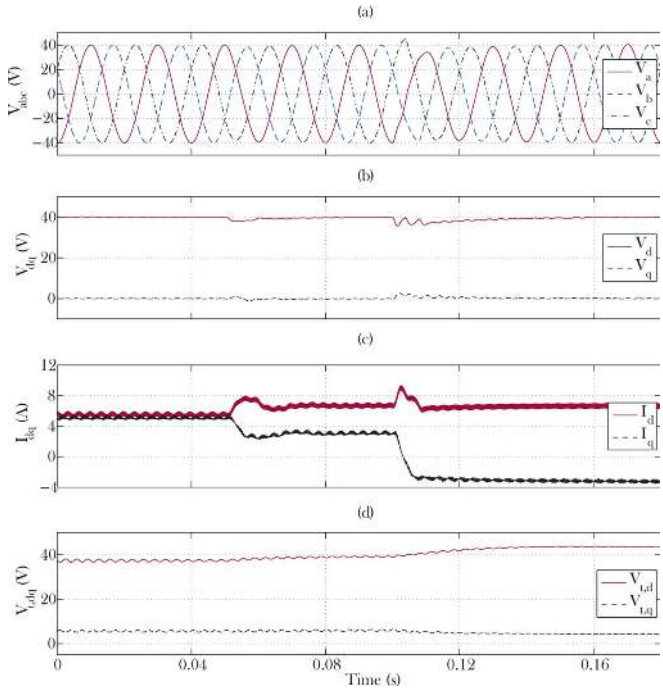

Fig. 9. The simulation response of the islanded system of Fig. 1 to the two-step inductive-capacitive load change of Fig. 6 when the MPRVC is in service: (a) the three-phase load voltages, (b), (c), and (d) the d- and q-components of the load voltages, the ac-side VSC currents, and the VSC terminal voltages.

subsequent to the linear resistive load changes. The comparison of Figs. 10(a) and 11(a) confirms the identical performance of the two controllers in the presence of linear loads. However, subsequent to the connection of the rectifier/nonlinear load at $t = 0.15$ s, the controllers behave differently. As shown in Fig. 10(a), upon the connection of the nonlinear load with the MPVC, significant low-order harmonics of order of 5 and 7 appear on the voltages, and the THD of the instantaneous load voltages increases significantly to about 12%. This is due to the inability of the MPVC to reject the harmonic disturbances. However, as Fig. 11(a) shows, the MPRVC is able to eliminate the 5th and 7th harmonics, and after a transient, the THD of the voltages remains within an acceptable range, i.e., less than 2%. Fig. 10(b)–(d) and Fig. 11(b)–(d) show the corresponding d- and q-components of the load voltages, the ac-side VSC currents, and the controllers outputs, when the MPVC and the MPRVC are in service, respectively. As depicted in Fig. 11(d), subsequent to the connection of the nonlinear load, the d- and q-components of the VSC terminal voltages, which are the control signals generated by the MPRVC, contain a ripple component with the frequency of 300 Hz. This ripple component is generated by the MPRVC to eliminate the harmonic voltage distortions generated by the rectifier load.

The simulation results of Fig. 11 highlight the capability of the MPRVC to eliminate the impacts of low-order harmonics and confirm its superior performance as compared with the MPVC in the presence of nonlinear loads. Furthermore, the expected decoupling between the dq-components of the load voltages, V_d and V_q, is observed from the simulation results of Figs. 8–11, which is a salient feature of the proposed MIMO controller, as compared with the one proposed in [25].

B. Experimental Results

The experimental evaluation and comparison of the performance of the proposed controllers are performed using an experimental test system with the same layout of the system of Fig. 1. The parameters of the experimental setup are set based on those given in Table I. The setup is loaded with the three-phase load configuration shown in Fig. 12. The proposed controllers are implemented in a fully digital control platform based on DSP/FPGA called *Boombox*, designed and developed in the Laboratory of Industrial Electronics at the EPFL, with a sampling frequency of up to 100 kHz. A photograph of the experimental setup, with highlighted main components, is shown in Fig. 13.

Initially, the system operates based on the MPVC, and the islanded test system is supplying a three-phase RLC load. The MPVC regulates the dq-components of the load voltages at 40 V and 0 V, respectively. At $t = 0.05$ s, as a nonlinear load, a three-phase full bridge rectifier with a 15 Ω resistive load is paralleled with the RLC load. Fig. 12 depicts the utilized load. Fig. 14 shows the dynamic response of the system in response to the rectifier energization. Fig. 14(a) and (b) depict the instantaneous load voltages and the VSC ac-side currents, respectively. Fig. 14(c) and (d) show the dq-components of the load voltages and the VSC ac-side currents, respectively. As opposed to the simulation results of Fig. 10, prior to the nonlinear load energization, the load voltages contain the 5th and 7th order harmonics, and have a THD of about 5.5%. This is due to the 4 μs dead-time of the VSC, which pollutes the VSC terminal voltages, and consequently, the VSC currents and the load voltages with low-order harmonics. This dead-time distortion is created dominantly by the 5th and the 7th order harmonics [34]. Subsequent to the nonlinear load energization, as shown in Fig. 14(b),

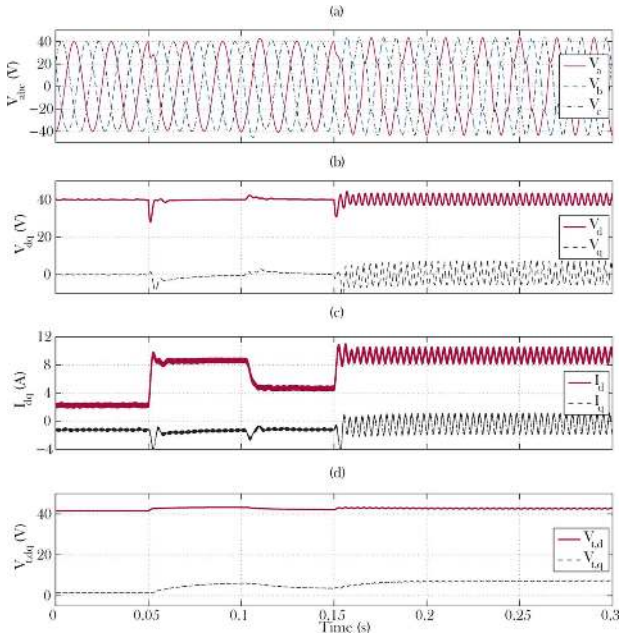

Fig. 10. The simulation response of the islanded system of Fig. 1 to the three-step resistive load change of Fig. 7 when the MPVC is in service: (a) the three-phase load voltages, (b), (c), and (d) the d- and q-components of the load voltages, the VSC ac-side currents, and the VSC terminal voltages.

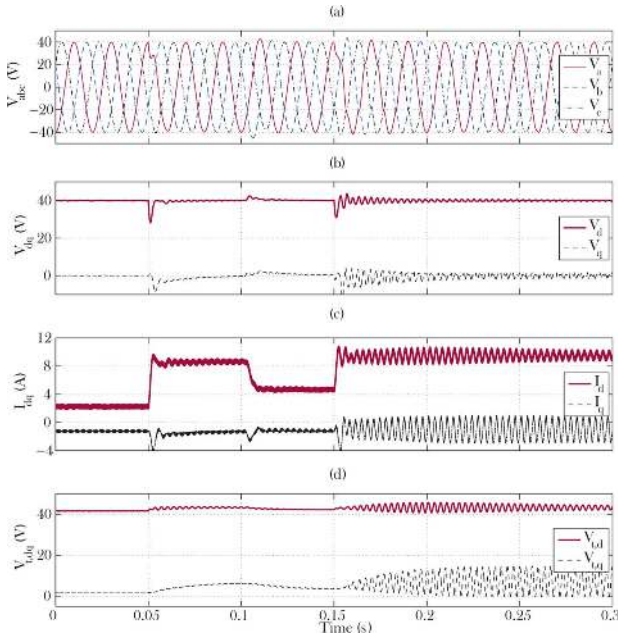

Fig. 11. The simulation response of the islanded system of Fig. 1 to the three-step resistive load change of Fig. 7 when the MPRVC is in service: (a) the three-phase load voltages, (b), (c), and (d) the d- and q-components of the load voltages, the VSC ac-side currents, and the VSC terminal voltages.

the VSC currents become distorted due to the rectifier operation, and consequently, the load voltages are further distorted, i.e., their THD increases to 15.5%. As expected, the MPRVC provides a unique capability to eliminate the adverse impacts of the harmonically polluting nonlinear loads. To demonstrate this capability, the same load change test is carried out when the system operates based on the MPRVC. Fig. 15 shows the dual waveforms of Fig. 14 when the MPRVC is in service. As Fig. 15(a) shows, prior to the nonlinear load energization, the load voltages, even with the dead-time effect, is harmonic free. This is due to the resonant terms of the MPRVC, which are tuned to, specifically, eliminate the harmonic components of the order of 5 and 7. Subsequent to the nonlinear load energization, due to the residual harmonic terms, the load voltages are slightly distorted. Nevertheless, the THD of the load voltages remains within the acceptable range, about 2.5%, which is due to the residual harmonic components of the order 11 and 13.

The experimental results of Figs. 14 and 15 show that both MIMO controllers successfully regulate the load voltages despite the imposed nonlinear dynamics. In addition, the MPRVC is able to counteract the adverse impacts of the low-order harmonic components and provide harmonic-free voltages.

VI. Conclusions

A multivariable digital design methodology for voltage control of a general VSC-based energy conversion system is proposed in this paper. The proposed methodology is based on shaping the open-loop MIMO transfer function matrix of the system by (i) attaining a family of nonparametric models of the system at various operating points, (ii) determining the class of the to-be-designed controller, and (iii) solving a convex optimization problem. The proposed controller design methodology is fully investigated in the context of voltage control of a single-DG-unit microgrid and its dedicated load.

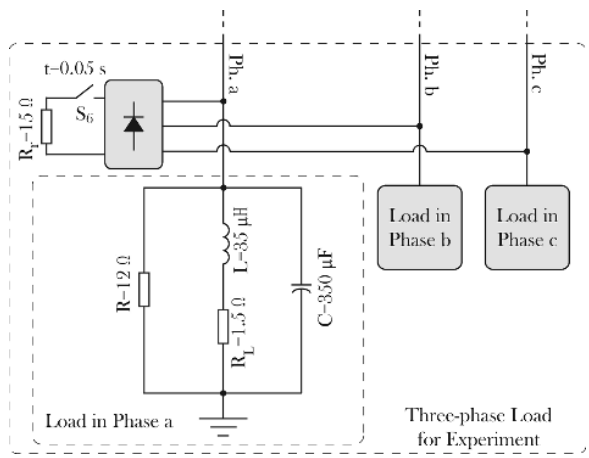

Fig. 12. The three-phase load for experimental investigation of resistive-load change scenarios.

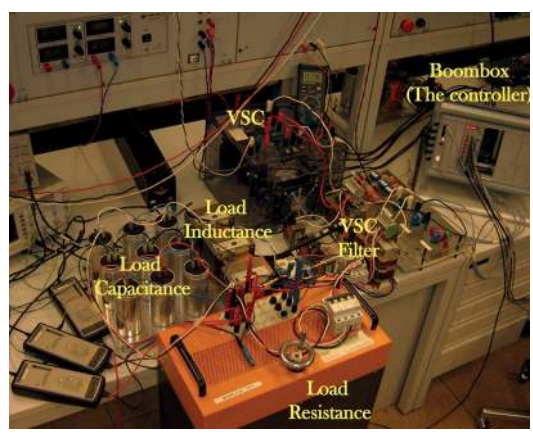

Fig. 13. The experimental setup.

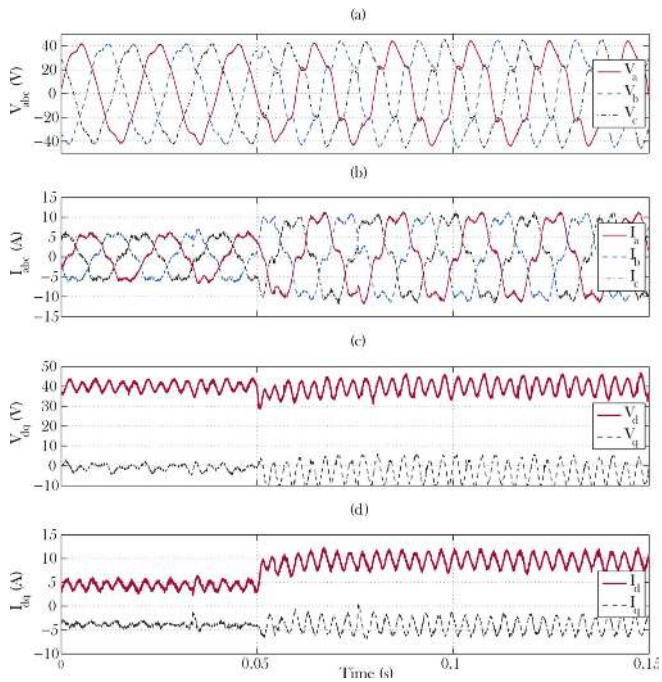

Fig. 14. The experimental response of the test system of Fig. 13 with respect to a nonlinear load energization when the MPVC is in service: (a),(b) the instantaneous load voltages and the VSC currents, and (c),(d) the d- and q-components of the load voltages and control signals.

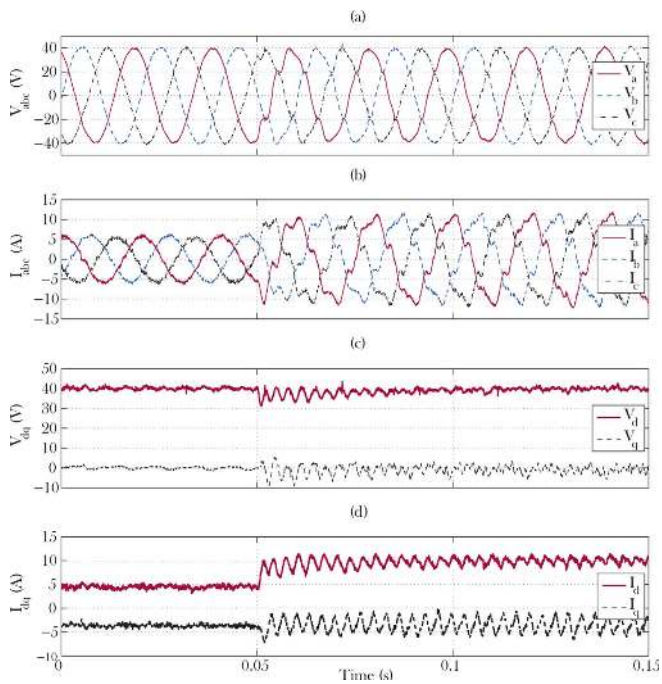

Fig. 15. The experimental response of the test system of Fig. 13 with respect to a nonlinear load energization when the MPRVC is in service: (a),(b) the instantaneous load voltages and the VSC currents, and (c),(d) the d- and q-components of the load voltages and control signals.

Two digital controllers are designed for the voltage regulation of the studied single-DG-unit microgrid system: (i) an MPVC and (ii) an MPRVC. The performance of the single-DG-unit microgrid system, based on the designed controllers, is evaluated for various operating scenarios. Based on the simulation and experimental results, the following conclusions are made:

- Both controllers show satisfactory dynamic performance in terms of load voltages regulation and robustness, upon step changes in linear loads.
- Compared with the MPVC, the MPRVC provides superior performance in the presence of nonlinear loads as it eliminates/minimizes the adverse impacts of the low-order harmonics on the load voltages and system operation.

Although the proposed voltage control strategies have been investigated for a single-DG-unit microgrid, they are applicable to a multi-DG-unit microgrid as well. In a multi-DG-unit microgrid, one of the DG units can act as a master controller. In such a case, the master DG-unit takes control over the voltage and frequency based on the proposed MPVC or MPRVC in this paper, and the rest of the DG units will be equipped with dq-currents controllers as if they are connected to the grid.

REFERENCES

[1] R. H. Lasseter, J. H. Eto, B. Schenkman, J. Stevens, H. Vollkommer, D. Klapp, H. Linton, and J. Roy, "CERTS microgrid laboratory test BeD," *IEEE Trans. Power Del.*, vol. 26, no. 1, pp. 325–332, Jan. 2011.

[2] B. Bahrani, S. Kenzelmann, and A. Rufer, "Multivariable-PI-based DQ current control of voltage source converters with superior Axes decoupling capability," *IEEE Trans. Ind. Electron.*, vol. 58, no. 7, pp. 3016–3026, Jul. 2011.

[3] B. Bahrani, A. Rufer, S. Kenzelmann, and L. A. C. Lopes, "Vector control of single-phase voltage-source converters based on fictive-axis emulation," *IEEE Trans. Ind. Applicat.*, vol. 47, no. 2, pp. 831–840, Mar./Apr. 2011.

[4] M. Liserre, R. Teodorescu, and F. Blaabjerg, "Multiple harmonics control for three-phase grid converter systems with the use of PI-RES current controller in a rotating frame," *IEEE Trans. Ind. Electron.*, vol. 21, no. 3, pp. 836–841, May 2006.

[5] H. Song and K. Nam, "Dual current control scheme for PWM converter under unbalanced input voltage conditions," *IEEE Trans. Ind. Electron.*, vol. 46, no. 5, pp. 953–959, Oct. 1999.

[6] B. K. Blyden and W. J. Lee, "Modified microgrid concept for rural electrification in Africa," presented at the IEEE Power and Energy Society General Meeting, 2006, PES GM'06.

[7] J. Balakrishnan, "Renewable energy and distributed generation in rural villages," in *Proc. 1st Int. Conf. on Industrial and Information Systems*, Aug. 2006, pp. 190–195.

[8] B. Bahrani, H. Karimi, and R. Iravani, "Nondetection zone assessment of an active islanding detection method and its experimental evaluation," *IEEE Trans. Power Del.*, vol. 26, no. 2, pp. 517–525, Apr. 2011.

[9] I. Balaguer-Alvarez, Q. Lei, S. Yang, U. Supatti, and Z. Peng, "Control for grid-connected and intentional islanding operations of distributed power generation," *IEEE Trans. Ind. Electron.*, vol. 58, no. 1, pp. 147–157, Jan. 2011.

[10] P. Piagi and R. H. Lasseter, "Autonomous control of microgrids," presented at the IEEE Power and Energy Society General Meeting, 2006, PES GM'06.

[11] I. A. Hiskens and E. M. Fleming, "Control of inverter-connected sources in autonomous microgrids," presented at the IEEE American Control Conference, Jun. 2008.

[12] F. Katiraei and R. Iravani, "Power management strategies for a microgrid with multiple distributed generation units," *IEEE Trans. Power Syst.*, vol. 21, no. 4, pp. 1821–1831, Nov. 2006.

[13] J. C. Vasquez, R. A. Mastromauro, J. M. Guerrero, and M. Liserre, "Voltage support provided by a droop-controlled multifunctional inverter," *IEEE Trans. Ind. Electron.*, vol. 56, no. 11, pp. 4510–4519, Nov. 2009.

[14] J. M. Guerrero, L. Hang, and J. Uceda, "Control of distributed uninterruptible power supply systems," *IEEE Trans. Ind. Electron.*, vol. 55, no. 8, pp. 2845–2859, Aug. 2008.

[15] J. M. Guerrero, J. C. Vasquez, J. Matas, L. G. de Vicuna, and M. Castilla, "Hierarchical control of droop-controlled AC and DC microgrids—A general approach towards standardization," *IEEE Trans. Ind. Electron.*, vol. 58, no. 1, pp. 158–172, Jan. 2011.

[16] J. C. Vasquez, J. M. Guerrero, A. Luna, P. Rodriguez, and R. Teodorescu, "Adaptive droop control applied to voltage-source inverters operating in grid-connected and islanded modes," *IEEE Trans. Ind. Electron.*, vol. 56, no. 10, pp. 4088–4096, Oct. 2009.

[17] R. Majumder, G. Ledwich, A. Ghosh, S. Chakrabarti, and F. Zare, "Droop control of converter-interfaced microsources in rural distributed generation," *IEEE Trans. Power Del.*, vol. 25, no. 4, pp. 2768–2778, Oct. 2010.
[18] J. M. Guerrero, J. C. Vasquez, J. Matas, L. G. de Vicuna, and M. Castilla, "Hierarchical control of droop-controlled DC and AC microgrids—A general approach towards standardization," *IEEE Trans. Ind. Electron.*, vol. 58, no. 1, pp. 158–172, Jan. 2011.
[19] J. M. Guerrero, L. G. de Vicuña, J. Matas, M. Castilla, and J. Miret, "A wireless controller to enhance dynamic performance of parallel inverters in distributed generation systems," *IEEE Trans. Power Electron.*, vol. 9, pp. 1205–1213, Sep. 2004.
[20] J. M. Guerrero, L. G. de Vicuña, J. Matas, M. Castilla, and J. Miret, "Output impedance design of parallel-connected UPS inverters with wireless load-sharing control," *IEEE Trans. Ind. Electron.*, vol. 52, pp. 1126–1135, Aug. 2005.
[21] J. M. Guerrero, J. Matas, L. G. de Vicuña, M. Castilla, and J. Miret, "Wireless-control strategy for parallel operation of distributed-generation inverters," *IEEE Trans. Ind. Electron.*, vol. 53, pp. 1461–1470, Oct. 2006.
[22] A. Mehrizi-Sani and R. Iravani, "Potential-function based control of a microgrid in islanded and grid-connected modes," *IEEE Trans. Power Syst.*, vol. 25, no. 4, pp. 1883–1891, Nov. 2010.
[23] C. K. Sao and P. W. Lehn, "Intentional islanded operation of converter fed microgrids," presented at the IEEE Power and Energy Society General Meeting, 2006, PES GM'06.
[24] M. B. Delghavi and A. Yazdani, "Islanded-mode control of electronically coupled distributed-resource units under unbalanced and nonlinear load conditions," *IEEE Trans. Power Del.*, vol. 26, no. 2, pp. 661–673, Apr. 2011.
[25] H. Karimi, H. Nikkhajoei, and R. Iravani, "Control of an electronically-coupled distributed resource unit subsequent to an islanding event," *IEEE Trans. Power Del.*, vol. 23, no. 1, pp. 493–501, Jan. 2008.
[26] H. Karimi, H. Nikkhajoei, and R. Iravani, "A linear quadratic Gaussian controller for a stand-alone distributed resource unit-simulation case studies," presented at the IEEE Power and Energy Society General Meeting, 2007, PES GM'07.
[27] H. Karimi, E. J. Davison, and R. Iravani, "Multivariable servomechanism controller for autonomous operation of a distributed generation unit: Design and performance evaluation," *IEEE Trans. Power Syst.*, vol. 25, no. 2, pp. 853–865, May 2010.
[28] H. Karimi, A. Yazdani, and R. Iravani, "Robust control of an autonomous four-wire electronically-coupled distributed generation unit," *IEEE Trans. Power Del.*, vol. 26, no. 1, pp. 455–466, Jan. 2011.
[29] J. M. Guerrero, J. Matas, L. Vicuña, M. Castilla, and J. Miret, "Decentralized control of parallel operation of distributed generation inverters using resistive output impedance," *IEEE Trans. Ind. Electron.*, vol. 54, no. 2, pp. 104–994, Apr. 2007.
[30] G. Galdos, A. Karimi, and R. Longchamp, "H_∞ controller design for spectral MIMO models by convex optimization," *J. Process Contr.*, vol. 20, no. 10, pp. 1175–1182, 2010.
[31] J. Doyle, B. Francis, and A. Tannenbaum, *Feedback Control Theory*. New York: Macmillan, 1990.
[32] I. D. Landau, R. Lozano, M. M'Saad, and A. Karimi, *Adaptive Control, Algorithms, Analysis and Applications*, 2nd ed. New York: Springer-Verlag, 2011.
[33] J. F. Strum, "Using SeDuMi 1.02, a Matlab toolbox for optimization over symmetric cones," *Optimization Methods and Software*, vol. 11, pp. 625–653, 1999.
[34] H. Kim, H. Moon, and M. Youn, "On-line dead-time compensation method using disturbance observer," *IEEE Trans. Power Electron.*, vol. 18, no. 6, pp. 1336–1345, Nov. 2003.

Behrooz Bahrani (S'07) received the B.Sc. degree from Sharif University of Technology, Tehran, Iran, the M.Sc. degree from the University of Toronto, Toronto, Canada, and the Ph.D. degree from Ecole Polytechnique Fédérale de Lausanne (EPFL), Lausanne, Switzerland, all in electrical engineering, in 2006, 2008, 2012, respectively.

From May to November 2008, he was a Research Intern at ABB Corporate Research, Dättwil-Baden, Switzerland. He is currently a Postdoctoral Fellow at the EPFL. His research interests include power electronics systems and their applications in power and traction networks.

Maryam Saeedifard (SM'11) received the Ph.D. degree in electrical engineering from the University of Toronto, Toronto, ON, Canada, in 2008.

Prior to joining Purdue University, West Lafayette, IN, she was a Visiting Research Associate with the Power Electronic Systems Group, ABB Corporate Research Center, Daettwil-Baden, Switzerland. Currently, she is an Assistant Professor in the School of Electrical and Computer Engineering, Purdue University. Her research interests include power electronics and applications of power electronics in power systems.

Dr. Saeedifard was the recipient of an NSERC Postdoctoral Fellowship of Government of Canada in 2008, and Richard M. Bass Outstanding Young Power Electronics Engineer Award of the IEEE Power Electronics Society in 2010.

Alireza Karimi (M'08) received his D.E.A. and Ph.D. degrees on Automatic Control from Institut National Polytechnique de Grenoble (INPG) in France in 1994 and 1997, respectively.

He was an Assistant Professor at Electrical Engineering Department of Sharif University of Technology, Tehran, Iran, from 1998 to 2000. He is currently a Senior Scientist at the Automatic Laboratory of Ecole Polytechnique Fédérale de Lausanne (EPFL), Lausanne, Switzerland. He serves as Associate Editor for the *European Journal of Control* since 2004. His research interests include robust control, adaptive control and data-driven controller tuning approaches.

Alfred Rufer (M'95–SM'01–F'06) received the M.Sc. degree from the Ecole Polytechnique Fédérale de Lausanne (EPFL), Lausanne, Switzerland, in 1976.

In 1978, he joined ABB, Turgi, Switzerland, where he was involved in the fields of power electronics and control, such as high-power variable frequency converters for drives, and where he was a Group Leader involved with power electronic development beginning in 1985. In 1993, he became an Assistant Professor at EPFL, where, since 1996, he has been a Full Professor and the Head of the Industrial Electronics Laboratory (LEI). LEI is active in power electronics used in energy conversion and energy storage and in the modeling and simulation of systems, including control strategies and control circuits. He has authored or coauthored many publications on power electronics and their applications, such as for multilevel converters or for different energy-storage systems. He is the holder of several patents.